

铝合金平板搅拌摩擦焊接应力变形分析

李红克, 史清宇, 王 鑫, 李 亭*

(清华大学机械工程系 先进成形制造教育部重点实验室, 北京 100084)

摘 要: 针对 6056-T6 铝合金平板进行搅拌摩擦焊接和试板变形检测试验。并用数值方法对试板变形进行模拟, 考察了模拟温度、应力场分布和试板变形情况, 对试验和模拟温度、变形进行比较。结果表明, 在文中条件下, 沿焊缝长度方向试板产生下挠, 最大变形量 6.3 mm; 沿试板宽度方向试板相对发生上拱, 最大变形量 4.5 mm, 模拟与实测变形趋势非常吻合。纵向残余应力在焊缝中心线两侧非对称性分布, 前进侧大于回转侧。

关键词: 搅拌摩擦焊; 焊接变形; 数值模拟

中图分类号: TG435 文献标识码: A 文章编号: 0253-360X(2008)02-0081-04



李红克

0 序 言

搅拌摩擦焊^[1] (friction stir welding, 简称 FSW) 是一种新型固相连接技术。由于材料在熔点以下温度实现成形与连接, 因而能够避免母材成分损失, 减少焊接缺陷, 保持力学性能^[2]。通常认为 FSW 可以获得较小残余应力和结构变形^[3]。但对较大尺寸薄板, 实际发现还是存在变形现象。因而, 开展 FSW 变形研究十分必要。而且, FSW 已进入工程结构应用阶段, 对结构可能产生的变形进行研究, 也是该技术的一个发展方向。尽管对于熔化焊接变形数值模拟已具有坚实的理论、实践基础^[4], 但对 FSW, 除存在与熔焊相似温度场作用外, 同时还存在较大外部压力、转矩作用。因而, 研究该技术特点下数值方法在焊接试板变形中的应用, 也是复杂工程结构变形模拟的必要前提和基础。

针对航空结构用 6056-T6 铝合金平板进行 FSW 试验, 检测并记录相关参数, 采用三坐标仪测量试板变形情况。同时利用数值方法模拟焊板温度、应力场及变形行为, 比较实测变形与模拟结果的差异, 为复杂结构 FSW 变形研究提供基础。

1 FSW 试验及变形测量

焊接材料 6056-T6, 单个焊板规格 400 mm × 150 mm × 3 mm。焊接起始及终了端各留 20 mm 未

焊, 焊缝总长 360 mm。搅拌工具轴肩直径 13 mm, 搅拌针直径 5 mm, 长 2.6 mm, 倾角 2°。被焊板材置于钢质垫板之上, 上部焊缝中心两侧施加 4 对固定约束, 装配如图 1 所示。工艺参数为: 转速 1 850 转/min, 焊速 700 mm/min, 焊接过程测量搅拌工具下压力和转矩, 同时在距焊缝一定位置处测量焊接过程温度。相关 FSW 试验在德国科隆 DLR 和 EADS 德国研究中心合作完成。

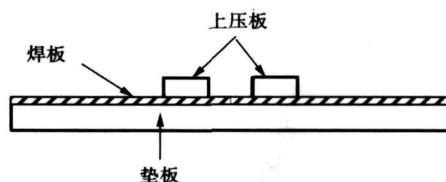


图 1 焊接装配示意

Fig 1 Assembly of panel and constraint plates

焊后试板在三坐标测量仪上进行变形检测。检测数据点呈网格分布, 网格间距 20 mm × 20 mm。

2 焊接变形数值模拟

2.1 数值模型

FSW 数值模拟采用 ABAQUS 商业软件建模。焊接温度场和应力变形以解耦方式计算。模型尺寸及组配与试验过程一致。对被焊铝板, 采用三维实体单元, 厚度方向划分两层。沿宽度方向划分单元时, 焊缝区采用较细的单元网格, 其他部位则采用粗

化及过渡网格。钢质垫板与上部压板则采用壳单元建立, 网格划分与被焊板材类似, 单元详细信息可参阅相关文献 [5]。模型及单元划分如图 2 所示。

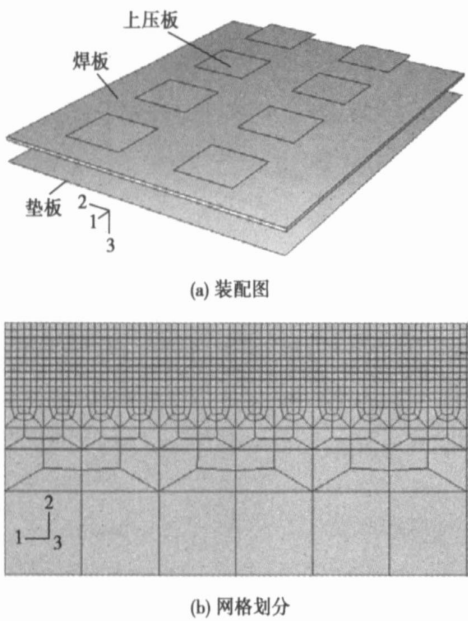


图 2 几何模型及网格划分
Fig. 2 Geometric model and mesh for welding panel and backing plate

2.2 焊接温度场计算

在稳定焊接阶段, 假设热输入为常数, 输入总热量可由搅拌工具转矩计算得到

$$Q = \eta \omega M = 2\pi \eta n M / 60 \quad (1)$$

式中: Q 为总热量, 单位 W; η 为功率系数, 这里设为 0.92; n 为搅拌工具转速, 单位 r/min; M 为转矩, 单位 N/m。

总热量被划分为轴肩面热源和搅拌针体热源两种形式分别施加于搅拌工具作用区域。搅拌针热量采用简化方法, 以总热量的 25% 计算^[6]。

温度场计算过程中主要边界条件为焊板底面与钢质垫板、上压板之间的接触热传导, 以及焊板、垫板、压板自由表面的对流散热。接触热传导系数与温度相关, 高温数据由低温数据点外推得到。对所有暴露在空气中的自由表面, 对流散热系数设定为 $15 \text{ W}/(\text{m}^2 \cdot ^\circ\text{C})$ 。

2.3 焊接应力场及变形计算

应力分析中外载荷主要包括搅拌工具下压力、转矩等。对下压力, 假设沿轴肩面均匀分布, 以平面压力表示。对转矩, 将其分解为工具区域下作用在单元 x, y 向的剪切分量, 由一定厚度下体力实现。面压力及体力通过子程序 DLOAD 加载。

应力变形分析中边界条件主要包括垫板支撑作用、上压板固定约束、侧边位移约束和在上述约束去除后为防止焊板刚性位移而施加的固定约束。

2.4 材料性能

模型所采用的材料性能由 EADS 德国研究中心提供, 如图 3, 图 4 所示。

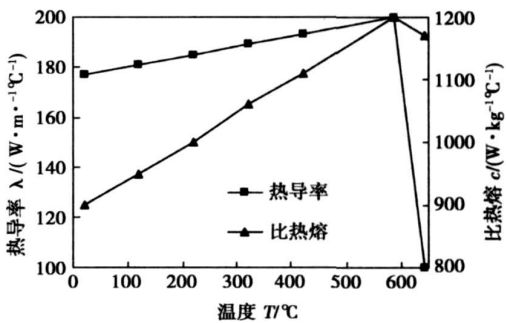


图 3 热导率和比热容与温度关系
Fig. 3 Thermo properties

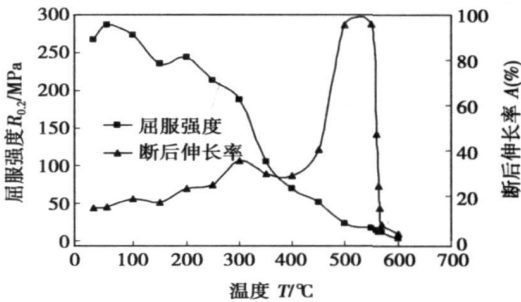


图 4 材料屈服强度和断后伸长率与温度关系
Fig. 4 Yield, tensile stress and elongation

3 结果与讨论

3.1 温度场模拟结果

焊接稳定阶段, 测量所得工具下压力和转矩平均值分别为 8.06 kN 和 8.76 N/m, 由此得到面热流及体热流密度为: $1171 \text{ W}/\text{m}^2$ 和 $390 \text{ W}/\text{m}^2$ 。在焊缝长度 200 mm 处焊缝中心位置, 模拟所得温度历程如图 5a 所示, 与峰值温度对应时刻沿焊缝横向的温度分布则如图 5b 所示。

图 5a 中, 温度—时间曲线呈突兀峰状分布, 最高温度 $462.5 \text{ } ^\circ\text{C}$ 。沿焊缝横向, 如图 5b, 随着距焊缝中心线距离的增加, 温度降低。但在 $l \leq 3.75 \text{ mm}$ 区域内形成一个高温台阶; 此后温度迅速降低, 最终在试板边缘处接近室温。

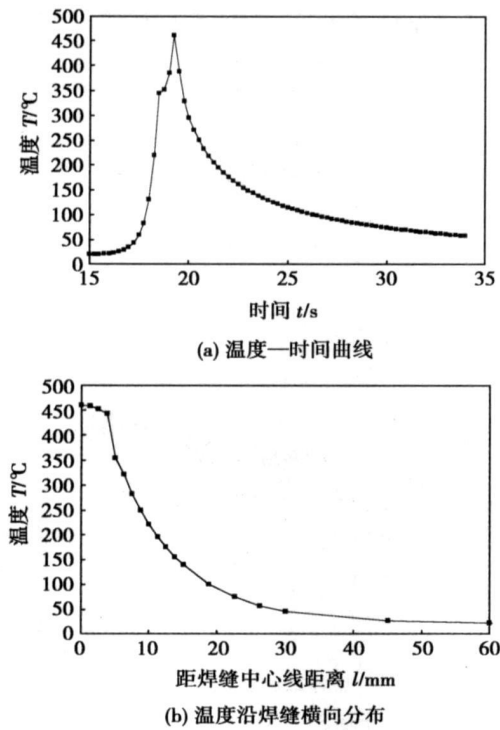


图 5 模拟温度分布
Fig 5 Simulated temperature distributions

对相同位置模拟和测量温度结果的分析表明, 在近焊缝区, 模拟温度稍高于测量温度, 在远离焊缝区, 测量温度稍高于模拟值, 但误差均 $<10\%$ 。

3.2 应力场模拟结果

在焊板长度 200 mm 处, 垂直于焊缝中心线处模拟所得纵、横向残余应力分布如图 6 所示。

可以看到, 在焊缝中心两侧各 10 mm 区域内, 纵向残余应力表现为较大的拉应力, 10 mm 以外则呈现为压应力。在拉应力区, 残余应力呈现不对称性分布, 前进侧拉应力高于回转侧。在焊缝两侧各 3.75 mm 处, 应力值分别为 269 和 247 MPa, 相差 22 MPa。这一现象与实测特点一致^[7]。焊缝两侧拉应力差异的出现是由于焊接过程热应力与机械应力叠加产生的结果。在前进侧材料承受机械拉应力, 而在回转侧则受到机械压应力作用, 二者与热应力复合即形成不对称分布。

在压应力区, 应力沿焊缝中心对称分布, 最大压应力为 37.1 MPa, 且随着距焊缝中心距离的增加, 应力值减小, 并在试板边缘达到最小值 9.6 MPa。

横向残余应力集中于焊缝中心及附近区域, 其性质与夹具约束有关, 这里主要表现为拉应力, 且沿焊缝中心线具有不对称性, 但差值很小。最大横向应力为 19.3 MPa, 位于前进侧搅拌针半径外缘。

对焊接试板长度中间位置、焊缝上、下表面纵向

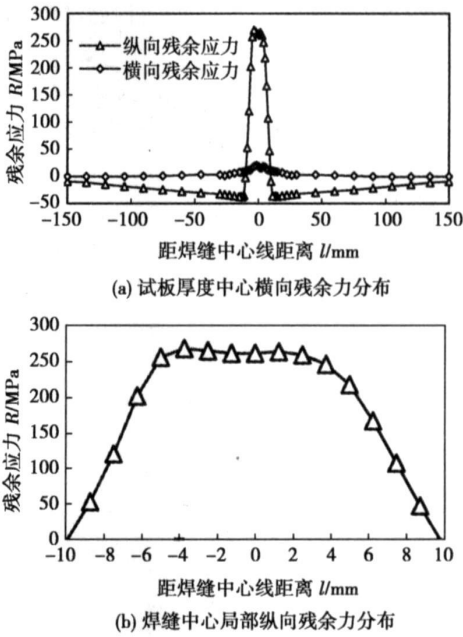


图 6 纵横向残余应力分布
Fig. 6 Longitudinal and transverse stress distributions

残余应力的分析表明, 在焊缝中心左右各 3.75 mm 区域内, 下表面拉应力大于上表面应力, 最大差值 27 MPa。但在试板无应力作用区域内, 上表面压应力大于下表面, 平均高出约 20 MPa。且在远离焊缝中心区域下表面纵向应力由压应力转变为拉应力, 并在试板边缘达到 11.4 MPa。

3.3 试板变形及模拟和测量结果比较

焊后试板变形及模拟所得变形情况如图 7 所示。其中图 7b 中网格为试板原始位置, 变形放大倍数为 5。实际焊板变形形式为: 沿焊缝长度方向, 试板整体形成下挠, 并在两侧边中心位置达到最大值。在焊缝横向, 试板出现上拱, 并在焊缝中心线达到高值。在图 7b 中, 模拟变形明显具有与实际焊板相同的变形趋势。

对 FSW 而言, 焊接变形的产生除与局部加热和快速冷却在焊缝及近缝区产生的热应变和压缩塑性应变相关外, 还与焊接过程外部机械载荷作用密不可分。塑性变形的产生进而导致内应力的出现, 最终形成构件的变形。

为进一步比较试验和模拟变形之间的差异, 将试板四边变形结果示于图 8。从中可见, 测量变形曲线出现交叉现象, 说明试板存在一定程度扭曲。扭曲的出现一方面为试板本身变形所致, 另一方面可能来源于变形测量误差。对于模拟结果, 四边位移曲线相对规律, 变形同样存在不对称性。在长度方向上, 前进侧边位移量同样大于回转侧, 但小于实

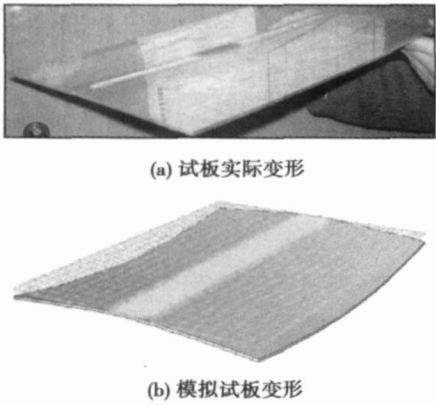


图 7 焊后试板变形与模拟变形

Fig. 7 Panel real and simulated distortions

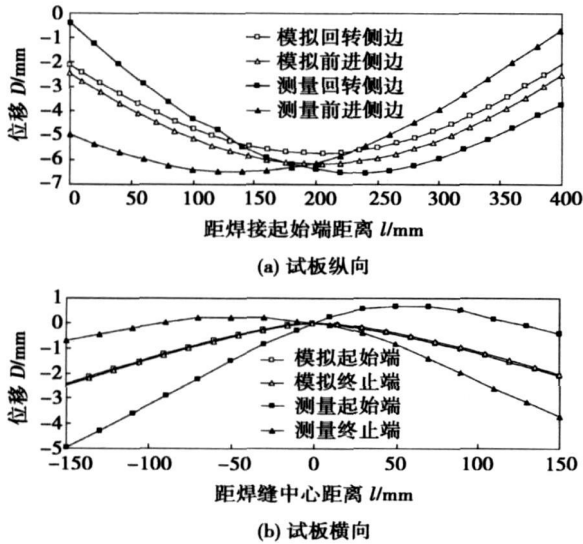


图 8 试板四边模拟变形与测量结果比较

Fig. 8 Distortion comparisons along panel edges for simulated and measured results

测变形量。

模拟变形与测量结果最大差异出现在试板四个角点, 差值在 1.68 ~ 2.51 mm 之间变化。在试板长度中间位置, 模拟结果接近或等于实际变形, 误差仅为 0.58 和 0.03 mm。

模拟变形与实测结果的差异主要来源于以下几个方面。(1)模拟温度场与实际存在 10 %左右的差异;(2)模型材料性能在高温阶段具有一定的不准确性, 尤其是高温应变数据为外推得到;(3)焊接过程中工具下压力和转矩随时间变化, 而模型中假设为

恒定机械载荷;(4)实际焊板两端各存在 20 mm 的未连接区域, 而数值模型未予考虑。

但从上述结果和分析可以发现, 采用数值方法模拟 FSW 试板和结构的变形可以获得一致的变形趋势。而且随着数值模型的改进, 模拟精度还可进一步提高, 因而对于指导 FSW 实践具有较大应用价值。

4 结 论

(1) FSW 焊后试板发生较大变形, 沿焊缝纵向, 试板形成下挠, 沿焊缝横向, 试板相对发生上拱。

(2) 利用数值方法, 可以实现对具有较大外部载荷条件下搅拌摩擦焊接试板变形情况的模拟, 并获得与实际焊板相一致的变形趋势。

(3) 搅拌摩擦焊接纵向残余应力在焊缝中心两侧呈不对称分布, 前进侧高于回转侧。

致 谢

研究项目得到 863 及 EADS 德国研究中心支持, 相关试验在德国合作完成。在此对参与该项目的德方 Jurgen Silvanus 先生表示衷心感谢。

参考文献:

[1] Thomas W M T, Nicholas E D, Need ham J C, *et al.* “Friction stir butt welding”: UK, International patent application no. PCT/GB92/02203 and GB patent application no. 9125978. 8[P]. 1991—12—01.

[2] Mishra R S, Ma Z Y. Friction stir welding and processing[R]. Materials Science and Engineering 2005, 50: 1—78.

[3] 栾国红, 关 桥. 高效、固相焊接新技术——搅拌摩擦焊[J]. 电焊机, 2005 35(9): 8—13.

[4] 蔡志鹏. 大型结构焊接变形的数值模拟研究与应用[D]. 北京: 清华大学, 2001.

[5] 李红克, 史清宇, 赵海燕, 等. 热量自适应搅拌摩擦焊热源模型[J]. 焊接学报, 2006, 27(11): 81—85.

[6] Shi Qingyu, Dickenson T, Shercliff H R. Thermo-mechanical analysis on welding process of aluminium 2024 with TIG and FSW[C]. // Proceedings of the 6th International Conference on Trends in Welding Research, 2003: 247—252.

作者简介: 李红克, 男, 1974 年出生, 博士研究生。主要从事搅拌摩擦焊接机理及数值模拟研究。发表论文 12 篇。

Email: hongkelee@163.com

under low heat input ZHANG Fujun¹, WANG Yan², ZHANG Guodong¹, Wang Yutao³ (1. College of Power & Mechanical Engineering, Wuhan University, Wuhan 430072, China; 2. College of Mechanical & Material Engineering, China Three Gorges University, Yichang 443002, Hubei, China; 3. Research Institute of Wuhan Iron & Steel Group Corporation, Wuhan 430080, China). p77—80

Abstract The formation and mechanical properties of welded joint for 400 MPa ultra-fine grain steel were studied based on surface tension transfer technology, CO₂ arc welding, special narrow groove and different heat input. The results showed that the welded joint with good fusion, one side welding with back formation and narrow HAZ (heat-affected zone) (about 1 mm) was obtained with 3–4 kJ/cm heat input. The hardness and tensile strength of the joint were higher than those of the base metal. The embrittlement and softening of HAZ was not found, and the bending plasticity was qualified. The impact toughness of HAZ was about 60% higher than that of the base metal, which can be caused by the granular pearlite transition, multi-phase non-equilibrium microstructure and higher yield stress.

Key words: ultra-fine grain steel; welded joint; heat input; CO₂ arc welding

Residual stress and distortion of Al alloy panels welded by FSW

LI Hongke, SHI Qingyu, WANG Xin, LI Ting, LIU Yuan (Department of Mechanical Engineering, Key Laboratory for Advanced Materials Processing Technology Ministry of Education, Tsinghua University, Beijing 100084, China). p81—84

Abstract FSW 6056-T6 Al alloy panel was welded by FSW and its distortion was measured. Also numerical model was established to simulate the distortion, temperature field and stress fields. The simulated temperature and distortion were compared with those of experiments. The results indicated that the panel bent down along welding direction and maximum distortion reaches 6.3 mm. Along the transverse direction, the panel bent up relatively to the longitudinal sides and the maximum displacement was 4.5 mm. There were high accordance trends of simulated distortion to the experiment. The longitudinal residual stress was asymmetric with the weld center line and it is higher on advancing side.

Key words: friction stir welding; welding distortion; numerical simulation

Microstructure and mechanical properties of K418 and 42CrMo dissimilar metal laser welding

PANG Ming, YU Gang, WANG Henghai, ZHENG Caiyun (Institute of Mechanics, Chinese Academy of Sciences, Beijing 100080, China). p85—88

Abstract The influences of welding heat input on weld of laser welding of K418 and 42CrMo dissimilar metal were experimentally investigated using continue wave Nd:YAG laser of output power 3 kW. Microstructure of the welded joint was studied by optical microscope, scanning electron microscope, X-ray diffraction, and energy dispersive spectrometer. Mechanical properties of the weld were

evaluated by hardness and tensile strength test. Results show that weld penetration of keyhole welding mode is larger than of heat conduction welding mode with constant linear heat input. Particle of rich Nb, Ti and Mo and deleted Fe and Ni and needle of rich Nb and Ti are observed in the fusion zone. The tensile strength of weld is higher than that of base metal of 42CrMo by optimizing laser welding parameters.

Key words: laser welding; heat-affected zone; K418 nickel alloy; 42CrMo steel; microstructure

Weld defect classification in ultrasonic testing basing on time-frequency discriminant features

DU Xiuli^{1,2}, SHEN Yi², WANG Yan² (1. School of Information Engineering, Dalian University, Dalian, 116622, China; 2. School of Astronautics, Harbin Institute of Technology, Harbin 150001, China). p89—92

Abstract According to transient property of ultrasonic signal, the discriminant pursuit method was proposed to extract local time-frequency features of defect signal and the features were fed to a probabilistic neural networks to classify the defects. During extracting features, the correlation between the incoming atom and the atoms selected before was considered to reduce the redundancy among the selected atoms so that the extracted features discriminated different class of signals effectively. Finally, the defects of an electronic welded joint were classified by proposed approach, and the experimental results show that time-frequency discriminant features are appropriate for defects classification in ultrasonic testing and can suppress the effect of grain noise. In addition, the higher accuracy can be reached if considering the correlation of the selected atoms.

Key words: ultrasonic test; discriminant pursuit; time-frequency discriminant feature; probabilistic neural networks

Prediction of area of gray-spots flaw in alternate rail flash butt welded joint based on RBF neural network

LÜQibing, TAN Keli, LUO Deyang, TAN Hongtao (Institute of Welding, Southwest Jiaotong University, Sichuan Chengdu 610031, China). p93—96

Abstract On the basis of imported AMS60 alternate rail flash butt welding machine, the welding current, the welding voltage and the displacement of welding procedure experiment of U71Mn rail were acquired with high frequency. Eight weld quality characteristic values such as the percentage of the flashing time of the accelerated flashing stage, the percentage of the flashing time of low voltage II and stable flash stage, the power input of weld, the flashed length of rail, the welding time, the short and broken circuit factor of low voltage II and stable flash stage and the short and broken circuit factor of the accelerated flashing stage and upsed length, which had influence on the grey-spot flaw area in the alternate rail flash butt welded joint, were used as input data of radial basic function neural network the rail weld grey-spot flaw. The prediction model whose spread rate was 1.5 was built, and according to the TB/T1632—